Propagation Characteristics of Rectangular Hermite-Gaussian Array Beams Through Oceanic and Atmospheric Turbulence

Hao Du, Guixuan Ding, Xing Du, Zhenyang Xiong, Sheng Wang, Qiang Liu, Hui Feng, and Simeng Wang

***Abstract*—This study investigates the propagation characteristics of rectangular Hermite-Gaussian array beams (RHGABs) through the oceanic and atmospheric turbulence considering ocean waves. Firstly, a theoretical model for the RHGABs in seawater-to-air propagation path is proposed. Secondly, we derive the expressions of the mean squared beam width and angular spread of RHGABs by using the extended Huygens-Fresnel principle and Rytov approximation. Finally, the effects of turbulent mediums on the RHGABs spreading are studied by analyzing the Rayleigh range. Our findings suggest that the Rayleigh range increases with the beam order of RHGABs. And the mean squared beam width of RHGABs in oceanic turbulence increases significantly higher than that in atmospheric turbulence. The results of this research can be applied to underwater optical communication systems.**

***Index Terms*—Atmospheric turbulence, cross-media, Hermite-Gaussian beam, oceanic turbulence, under water optical communication.**

I. Introduction

IN THE past decades, underwater laser communications have gained attention due to their advantages over traditional wireless transmission methods, including higher bandwidth, lower time latency, and enhanced security [1]. The high-order Gaussian beam and orbital angular momentum (OAM) in underwater laser communications has been widely studied [2], [3], [4], [5]. In practical maritime communication systems, as represented in Fig. 1, information can be transmitted from submarines to aircraft through the seawater-to-air link [6]. Consequently, the research on the propagation characteristics of laser beams through oceanic and atmospheric turbulence has become a key hotspot, particularly in cross-media scenarios.

Currently, using high-order beam and multi-beams are common solutions for resisting the effects of turbulence [7], [8], [9], [10], [11], [12], [13], [14], [15], [16]. Particularly, Hermite-Gaussian array beams (HGABs), as a kind of topical high-order beams, have been shown to be less sensitive to turbulence than Gaussian beams [12], [13]. Wang derived an analytical expression for the propagation factors of partially coherent elegant Hermite-cosh Gaussian beams in non-Kolmogorov [14]. Sayan examined the propagation distances and the zenith angles at the realistic propagation distances involved in uplink and downlink configurations [15]. Yuan studied the evolution properties of the M^2 factor of the Hermite–Gaussian beam in turbulent atmosphere [16]. Zhu derived the propagation formula of the radially polarized Hermite-cos-Gaussian correlated Schell-model beam in oceanic turbulence [17]. Li established the model of the received probability density of orbital angular momentum (OAM) modes of a new Hermite-Gaussian vortex beam propagating through the turbulent ocean of anisotropy [16]. Zhou derived the analytically general expressions of the centroid and the beam spot size of an elegant Hermite-Gaussian beam passing through an Airy transform optical system [19]. Wu studied the evolution behavior of Hermite-cosine-Gaussian beam propagating in oceanic turbulence [20]. Additionally, the rectangular Gaussian array beams are widely used in various fields, such as high-power systems and inertial confinement fusion [21]. Therefore, we aim to study the beam quality of rectangular Hermite-Gaussian beams propagating through the oceanic and atmospheric turbulence.

Recently, a massive number of studies have been done on the laser beam propagating in atmospheric and oceanic turbulence separately [14], [15], [16], [17], [18], [19], [20], [21], [22], [23], [24], [25], [26], [27]. The intensity fluctuations, beam wander, beam width of Hermite-Gaussian beams and Gaussian beams in turbulent mediums have been studied. These researches, however, have primarily focused on the single transmission mediums, with relatively little research on laser beam propagating through the oceanic and atmospheric turbulence continuously. To address this gap, we propose a universal model

Manuscript received 29 June 2023; revised 9 August 2023; accepted 18 August 2023. Date of publication 24 August 2023; date of current version 4 September 2023. This work was supported in part by the Natural Science Foundation of Hainan Province under Grants 622MS105 and 620MS076, and in part by the Youth Innovation Promotion Association of Chinese Academy of Sciences under Grant 2020133. *(Hao Du and Guixuan Ding are co-first authors.) (Corresponding author: Xing Du.)*

Hao Du is with the Aerospace Information Research Institute, Chinese Academy of Sciences, Beijing 100094, China, and also with the Key Laboratory of Earth Observation of Hainan Province, Hainan Aerospace Information Research Institute, Wenchang 571300, China.

Guixuan Ding, Xing Du, Zhenyang Xiong, Sheng Wang, and Qiang Liu are with the Aerospace Information Research Institute, Chinese Academy of Sciences, Beijing 100094, China, and also with the University of Chinese Academy of Sciences, Beijing 101408, China (e-mail: duxing20@mails.ucas.ac.cn).

Hui Feng is with the Aerospace Information Research Institute, Chinese Academy of Sciences, Beijing 100094, China, also with the University of Chinese Academy of Sciences, Beijing 101408, China, and also with the Key Laboratory of Earth Observation of Hainan Province, Hainan Aerospace Information Research Institute, Wenchang 571300, China.

Simeng Wang is with the Aerospace Information Research Institute, Chinese Academy of Sciences, Beijing 100094, China.

Digital Object Identifier 10.1109/JPHOT.2023.3308074

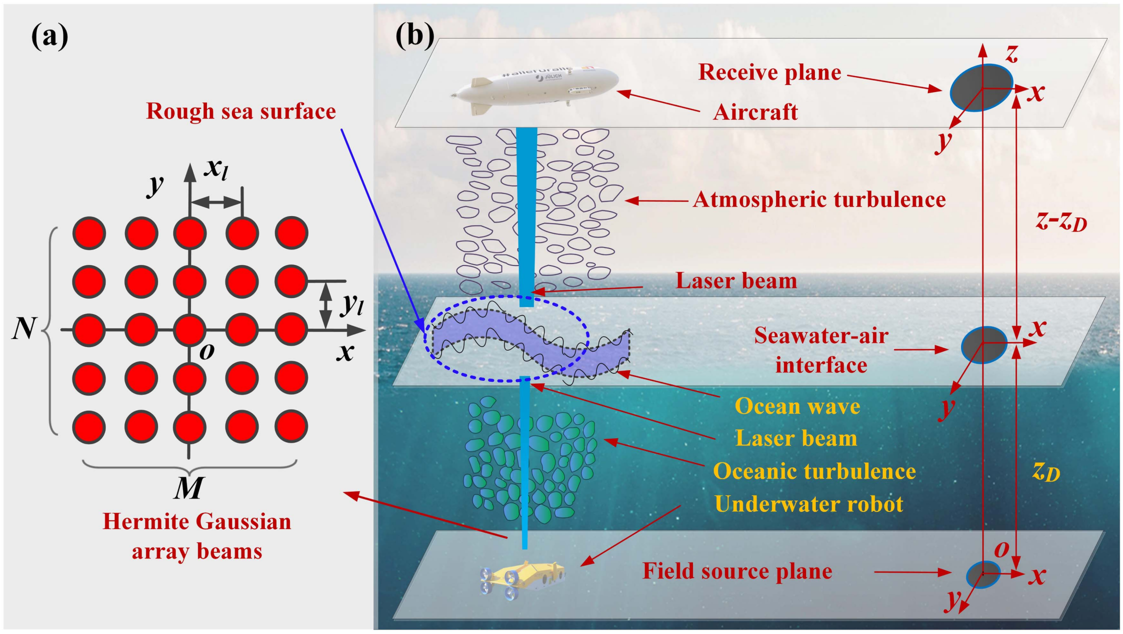

Fig. 1. Diagram of laser beams propagating through seawater-to-air.

for RHGABs propagation in cross-media paths, building on the past researches.

Our research employs the Rytov approximation and extended Huygens-Fresnel principle to model the light field propagation through the seawater-to-air path. Moreover, we derive expressions for parameters such as mean squared beam width, angular spread, and Rayleigh range, which reflect the characteristics of beam propagation.

The rest structure of this paper is organized as follows: in Section II, the analytical analyses of the beam transmission properties are given. In Section III, the numerical results are analyzed. And the conclusions are drawn in Section IV.

II. Theoretical Analysis

A. Light Field Propagating Though Double Turbulent Mediums

It can be illustrated from Fig. 1 that the light field in receptive plane is determined by the initial light field, the refractive index fluctuations caused by the turbulent mediums and rough sea surface. In our model, the rough sea surface is considered as a medium combined by the ocean, atmosphere, and interface, which is discussed separately. Noting the beam intensity attenuation at the rough sea surface. We consider the transmittance of RHGABs propagating through the seawater-air interface, which is denoted as Ξ.

First, the light field propagating in free space is obtained by the extended Huygens-Fresnel principle, which can be written as [28]

$$U^{(free)}(x,y,z) = -\frac{ik\mathrm{e}^{ikz}}{2\pi z}\iint dx_0dy_0U_0(x_0,y_0,0) \times \exp\left\{\frac{ik}{2z}\left[(x-x_0)^2+(y-y_0)^2\right]\right\} \quad (1)$$

where k is the wave number, $U^{(free)}$ (x, y, z) is the field intensity at (x, y, z), U_0 $(x_0, y_0, 0)$ denotes the field intensity of the point $(x_0, y_0, 0)$ in the field source plane (initial plane).

Second, we can obtain the light field in individual turbulent medium according to Rytov approximation [28], i.e.,

$$U^{(t)}(x,y,z) = U^{(free)}(x,y,z)\,\ell_A^{(1)}\ell_A^{(2)}\ell_A^{(3)}\cdots \quad (2)$$

where $U^{(t)}$ denotes the light field in an individual turbulent medium, $U^{(free)}$ is the light field in the free space, $\ell_A^{(i)}$ denotes the ith order complex phase perturbation caused by turbulence.

Third, considering the light field transmitting through double turbulent mediums (A and B) continuously, and neglecting the higher-order terms, (2) is rewritten as

$$U^{(tt)}(x,y,z) = \begin{cases} U^{(free)}(x,y,z)\,\ell_A^{(1)}, & \text{transmitting in A} \\ U^{(free)}(x,y,z)\,\ell_A^{(1)}\ell_B^{(1)}, & \text{transmitting in B} \end{cases} \quad (3)$$

where $U^{(tt)}$ denotes the light field propagating in double turbulent mediums, $\ell_B^{(i)}$ denotes the ith order complex phase perturbation caused by the second turbulent medium.

In practice, as mentioned in Fig. 1, the (3) is applied in the seawater-to-air propagation path. And since the complex phase $\ell_A^{(i)}$ and $\ell_B^{(i)}$ are determined by the spatial coordinates, the complex phase perturbations mentioned in (3) can be written as [28]

$$\ell_A^{(1)} = \ell_{ocean}^{(1)} = \exp\left[\psi^{(o)}(\boldsymbol{r}_a,\boldsymbol{r}_1,l)\right] \quad (4)$$

$$\ell_B^{(1)} = \ell_{air}^{(1)} = \exp\left[\psi^{(a)}(\boldsymbol{r}_a,\boldsymbol{r}_1,l)\right] \quad (5)$$

where, $\boldsymbol{r}_a = (x, y)$, $\boldsymbol{r}_1 = (r_{x1}, r_{y1})$, l denotes the propagation distance.

Then, upon substituting (1), (4), (5) to (3), we can obtain

$$U^{(tt)}(x,y,z)=\begin{cases}-\frac{ike^{ikz}}{2\pi z}\int\int dx_0dy_0U_0(x_0,y_0,0)\\ \times\exp\{\frac{ik}{2z}[(x-x_0)^2+(y-y_0)^2]\}\\ \times\exp[\psi^{(o)}(\boldsymbol{r}_\alpha,\boldsymbol{r}_1,z)],(0\le z\le z_D)\\ -\frac{ike^{ikz}}{2\pi z}\int\int dx_0dy_0U_0(x_0,y_0,0)\\ \times\exp\{\frac{ik}{2z}[(x-x_0)^2+(y-y_0)^2]\}\\ \times\exp[\psi^{(o)}(\boldsymbol{r}_\alpha,\boldsymbol{r}_1,z_D)]\\ \times\exp[\psi^{(a)}(\boldsymbol{r}_\alpha,\boldsymbol{r}_1,z-z_D)],\\ (z_D<z)\end{cases}\tag{6}$$

where z_D is the distance from the initial plane to seawater-air interface, z is the distance from receiving plane to initial plane.

Here, RHGABs are composed of $M\times N$ equal Hermite-Gaussian beams. As shown in Fig. 1(a), the distance between two adjacent Hermite-Gaussian array beams in the x, y axis direction is x_l, y_l, respectively. The field distribution ($z=0$) of the off-axis RHGABs centered at point (ix_d, jy_d), reads as [29]

$$U_{ij}(x_0,y_0,0)=U_i(x_0,0)U_j(y_0,0)\tag{7}$$

$$U_i(x_0,0)=e^{-\frac{(x_0-ix_l)^2}{w_0^2}}H_m\left[\frac{\sqrt{2}(x_0-ix_l)}{w_0}\right],\quad i\in\left[-\frac{M-1}{2},\frac{M-1}{2}\right],\tag{8}$$

$$U_j(y_0,0)=e^{-\frac{(y_0-jy_l)^2}{w_0^2}}H_n\left[\frac{\sqrt{2}(y_0-jy_l)}{w_0}\right],\quad j\in\left[-\frac{N-1}{2},\frac{N-1}{2}\right],\tag{9}$$

where, $H_m(\bullet)$ and $H_n(\bullet)$ are the mth and nth order Hermite polynomials, respectively. And m and n are abbreviation for beam order in the following. Particularly, the RHGABs can be regard as Gaussian array beams (GABs) if the order $m=n=0$.

Thus, we can obtain the field intensity of the point (x_0, y_0, 0) in the field source plane, which can be written as

$$U_0(x_0,y_0,0)=\sum_i\sum_j U_{ij}(x_0,y_0,0)\tag{10}$$

We assume that the RHGABs are correlated, and the cross-spectral density function (CSDF) of the RHGABs can be written as

$$W(\boldsymbol{r}_{a1},\boldsymbol{r}_{a2},z)=U^{(tt)}(\boldsymbol{r}_{a1},z)U^{(tt)^*}(\boldsymbol{r}_{a2},z)\tag{11}$$

where the $U^{(tt)}*$ denotes the complex conjugate of $U^{(tt)}$.

B. Intensity Calculation in Seawater to Air Propagation Path

Assuming $\boldsymbol{r}_{a1}=\boldsymbol{r}_{a2}=\boldsymbol{r}$, the light intensity in the receiving plane ($z>z_D+d_\varepsilon$) can be represented as (12). Noting that the expression of light intensity when $z\le z_D$ is similar to (12), which is not listed here.

$$\begin{aligned}I(\boldsymbol{r},z)&=W(\boldsymbol{r},\boldsymbol{r},z)\\&=\left(\frac{k}{2\pi z}\right)^2\iint\iint d^2\boldsymbol{r}_1d^2\boldsymbol{r}_2W^{(0)}(\boldsymbol{r}_1,\boldsymbol{r}_2,0)\\&\times\exp\left\{\frac{ik}{2z}\left[(\boldsymbol{r}-\boldsymbol{r}_1)^2-(\boldsymbol{r}-\boldsymbol{r}_2)^2\right]\right\}\\&\times\left\langle\exp\left[\psi^{(ocean)}(\boldsymbol{r},\boldsymbol{r}_1,z_D)+\psi^{(ocean)*}(\boldsymbol{r},\boldsymbol{r}_2,z_D)\right]\right\rangle_m\\&\times\left\langle\exp\left[\psi^{(air)}(\boldsymbol{r},\boldsymbol{r}_1,z-z_D)+\psi^{(air)*}(\boldsymbol{r},\boldsymbol{r}_2,z-z_D)\right]\right\rangle_m\end{aligned}\tag{12}$$

where $\psi(\bullet)$ denotes the random part of the complex phase due to the turbulence. $<\bullet>_m$ represents the average over the ensemble of the turbulent medium, and it can be written as [9], [30]

$$\begin{aligned}&\left\langle\exp\left\{\psi^{(ocean)}(\boldsymbol{r},\boldsymbol{r}_1,z_D)+\psi^{(ocean)*}(\boldsymbol{r},\boldsymbol{r}_2,z_D)\right\}\right\rangle_m\\&=\exp\left\{-4\pi^2k^2z\int_0^1\int_0^\infty\kappa\Phi_n^{(ocean)}(\kappa)\times[1-J_0(\kappa\xi|\boldsymbol{r}_2-\boldsymbol{r}_1|)]d\kappa d\xi\right\}\end{aligned}\tag{13}$$

$$\begin{aligned}&\left\langle\exp\left[\psi^{(air)}(\boldsymbol{r},\boldsymbol{r}_1,z-z_D)+\psi^{(air)*}(\boldsymbol{r},\boldsymbol{r}_2,z-z_D)\right]\right\rangle_m\\&=\exp\left\{-4\pi^2k^2(z-z_D)\int_0^1\int_0^\infty\kappa\Phi_n^{(air)}(\kappa)\times[1-J_0(\kappa\xi|\boldsymbol{r}_2-\boldsymbol{r}_1|)]d\kappa d\xi\right\}\end{aligned}\tag{14}$$

where the $\Phi_n(\kappa)$ denotes the spatial power spectrum of the turbulent refractive-index fluctuations, κ is the magnitude of spatial wave number. $J_0(\bullet)$ is the Bessel function of the first kind and order zero [9].

The power spectrum for homogeneous and isotropic oceanic water when the eddy thermal diffusivity equal to the diffusion of salt is read as [5]

$$\Phi_n^{(ocean)}(\kappa)=0.388\times10^{-8}\varepsilon^{-1/3}\kappa^{-11/3}\left[1+2.35(\kappa\eta)^{2/3}\right]\frac{\chi_T}{w^2}\left(w^2e^{-A_T\delta}+e^{-A_S\delta}-2we^{-A_{TS}\delta}\right),\tag{15}$$

where ε is the rate of dissipation of turbulent kinetic energy per unit mass of fluid, which may vary in range from 10^{-1} m^2/s^3 to 10^{-10} m^2/s^3, η (inner scale), and with χ_T being the rate of dissipation of mean-square temperature, taking values in the range from 10^{-2} K^2/s in surface water to 10^{-10} K^2/s in deep water, $A_T=1.863\times10^{-2}$, $A_S=1.9\times10^{-4}$, $A_{TS}=9.41\times10^{-3}$, and $\delta=8.284(\kappa\eta)^{4/3}+12.978(\kappa\eta)^2$. w is the parameter that determines the relative strength of temperature and salinity in driving the index fluctuations [−5; 0] [9].

The power spectrum for atmospheric turbulence is represented as (16), by using the non-Kolmogorov spectrum [30]

$$\Phi_n^{(air)}(\kappa)=A(\alpha)\tilde{C}_n^2\exp\left(-\kappa^2/\kappa_m^2\right)\left(\kappa^2+\kappa_0^2\right)^{-\alpha/2},\quad 0<\kappa<\infty,\quad 3<\alpha<4,\tag{16}$$

where $A(\alpha) = \Gamma(\alpha–1)\cos(\alpha\pi/2)/(4\pi^2)$, $\kappa_0 = 2\pi/L_0$, and $\kappa_m = c(\alpha)/l_0$, in which $c(\alpha) = \{\Gamma[(5–\alpha)/2] \cdot A(\alpha) \cdot 2\pi/3\}^{1/(\alpha-5)}$, L_0 is the outer scale, and l_0 is the inner scale.

Here, we assume $\boldsymbol{u} = (\boldsymbol{r}_1 + \boldsymbol{r}_2)/2$, $\boldsymbol{v} = \boldsymbol{r}_2 - \boldsymbol{r}_1$, recalling the transmittance (Ξ) of RHGABs through seawater-air interface. Where, Ξ denotes the ratio of transmitted light intensity to incident light intensity.

Thus, we have

$$I^{(\mathrm{out})}(\boldsymbol{r}, z) = \Xi \cdot I^{(\mathrm{in})}(\boldsymbol{r}, z) \tag{17}$$

where, $I^{(\mathrm{out})}(\boldsymbol{r}, z)$ denotes the beam intensity after the reflection and absorption in the interface, $I^{(\mathrm{in})}(\boldsymbol{r}, z)$ denotes the beam intensity before the reflection and absorption in the interface. Therefore, the average intensity of the RHGABs represented by (12) propagating in the whole propagation path reads as

$$I(\boldsymbol{r}, z) = \begin{cases} \left(\frac{k}{2\pi z}\right)^2 \iint \mathrm{d}^2\boldsymbol{u} \iint \mathrm{d}^2\boldsymbol{v} W(\boldsymbol{u}, \boldsymbol{v}, 0) \\ \quad \times \exp\left(-\frac{\mathrm{i}k}{z}\boldsymbol{u}\cdot\boldsymbol{v}\right) \exp\left(\frac{\mathrm{i}k}{z}\boldsymbol{r}\cdot\boldsymbol{v}\right) \\ \times \exp\left\{-4\pi^2k^2 z \int_0^1 \int_0^\infty \kappa \Phi_n^{(ocean)}(\kappa) \right. \\ \quad \left. [1 - J_0(\kappa\xi\boldsymbol{v})]\,\mathrm{d}\kappa \mathrm{d}\xi\right\}, \\ 0 \le z \le z_D \\ \\ \left(\frac{k}{2\pi z}\right)^2 \iint \mathrm{d}^2\boldsymbol{u} \iint \mathrm{d}^2\boldsymbol{v} W(\boldsymbol{u}, \boldsymbol{v}, 0) \\ \quad \times \exp\left(-\frac{\mathrm{i}k}{z}\boldsymbol{u}\cdot\boldsymbol{v}\right) \exp\left(\frac{\mathrm{i}k}{z}\boldsymbol{r}\cdot\boldsymbol{v}\right) \\ \times \exp\left\{-4\pi^2k^2 z \int_0^1 \int_0^\infty \kappa \right. \\ \quad \left[\Xi\left(\gamma_1 + \gamma_2\frac{z_D + d_\varepsilon/2}{z}\right)\Phi_n^{(ocean)}(\kappa)\right. \\ \quad \left.\left. + \gamma_2 \frac{(z - z_D - d_\varepsilon/2)}{z}\Phi_n^{(air)}(\kappa)\right][1 - J_0(\kappa\xi\boldsymbol{v})]\,\mathrm{d}\kappa \mathrm{d}\xi\right\}, \\ z_D < z \le z_D + d_\varepsilon \\ \\ \left(\frac{k}{2\pi z}\right)^2 \iint \mathrm{d}^2\boldsymbol{u} \iint \mathrm{d}^2\boldsymbol{v} W(\boldsymbol{u}, \boldsymbol{v}, 0) \times \exp\left(-\frac{\mathrm{i}k}{z}\boldsymbol{u}\cdot\boldsymbol{v}\right) \\ \exp\left(\frac{\mathrm{i}k}{z}\boldsymbol{r}\cdot\boldsymbol{v}\right) \\ \times \exp\left\{-4\pi^2k^2 z \int_0^1 \int_0^\infty \kappa[\Xi\frac{z_D + d_\varepsilon/2}{z}\Phi_n^{(ocean)}(\kappa)\right. \\ \left. + \frac{(z - z_D - d_\varepsilon/2)}{z}\Phi_n^{(air)}(\kappa)]\,[1 - J_0(\kappa\xi\boldsymbol{v})]\,\mathrm{d}\kappa \mathrm{d}\xi\right\}, \\ \quad z_D + d_\varepsilon < z \end{cases} \tag{18}$$

where, γ_1 is the probability of the laser propagation in the oceanic turbulence, γ_2 is the probability of the laser propagation in the atmospheric turbulence, d_ε is the thickness of the wave layer. And we assume $\gamma_1 = 1 – \Phi\ (z - z_d - d_\varepsilon/2)$, $\gamma_2 = 1 - \gamma_1$, $\Phi\ (\bullet)$ denotes the distribution function of the Gaussian distribution.

C. Mean Squared Beam Width and Angular Spread

The mean-squared beam width is written as [31]

$$w^2(z) = \frac{4\iint \boldsymbol{\rho}^2 \langle I(\boldsymbol{r}, z)\rangle \mathrm{d}x\mathrm{d}y}{\iint \langle I(\boldsymbol{r}, z)\rangle \mathrm{d}x\mathrm{d}y} \tag{19}$$

Upon substitution (17) to (19). It is easy to find that

$$w^2(z)\big|_{\mathrm{in}} = \frac{4\iint \boldsymbol{\rho}^2 \langle I(\boldsymbol{r}, z)^{(\mathrm{in})}\rangle \mathrm{d}x\mathrm{d}y}{\iint \langle I(\boldsymbol{r}, z)^{(\mathrm{in})}\rangle \mathrm{d}x\mathrm{d}y} \tag{20}$$

$$w^2(z)\big|_{\mathrm{out}} = \frac{4\iint \boldsymbol{\rho}^2 \langle I(\boldsymbol{r}, z)^{(\mathrm{out})}\rangle \mathrm{d}x\mathrm{d}y}{\iint \langle I(\boldsymbol{r}, z)^{(\mathrm{out})}\rangle \mathrm{d}x\mathrm{d}y} \tag{21}$$

$$w^2(z)\big|_{\mathrm{out}} = w^2(z)\big|_{\mathrm{in}} \tag{22}$$

It means that, the mean squared beam width is not affect by the reflection and absorption in the seawater-air interface.

Upon substituting (18) to (19), and after straight calculation, we can obtain

$$w^2(z) = (\alpha_x + \alpha_y) + \frac{\beta_x + \beta_y}{k^2} z^2 + \Theta z^3, \tag{23}$$

where

$$\alpha_{x,y} = \sum_{i_1 = -\frac{M-1}{2}}^{\frac{M-1}{2}} \sum_{i_2 = \frac{M-1}{2}}^{\frac{M-1}{2}} \exp(-D/2) \times \left\{w_0^2\left[L_m(D) - 2L_m^{(1)}(D)\right] + (i_1 + i_2)^2 x_d^2 L_m(D)\right\}/2C \tag{24}$$

$$\beta_{x,y} = \sum_{i_1 = -\frac{M-1}{2}}^{\frac{M-1}{2}} \sum_{i_2 = -\frac{M-1}{2}}^{\frac{M-1}{2}} 2\exp(-D/2) \times \left\{L_m(D) - 2L_m^{(1)}(D) - \left[L_m(D) - 4L_m^{(1)}(D) + 4L_m^{(2)}(D)\right] D\right\}/w_0^2 C, \tag{25}$$

$$D = (i_1 - i_2)^2 x_d^2 / w_0^2 \tag{26}$$

$$C = \sum_{i_1 = -\frac{M-1}{2}}^{\frac{M-1}{2}} \sum_{i_2 = -\frac{M-1}{2}}^{\frac{M-1}{2}} \exp(-D/2) L_m(D) \tag{27}$$

$$\Theta = \begin{cases} \frac{8}{3}\pi^2 \int_0^\infty \kappa^3 \left[\Phi_n^{(ocean)}(\kappa)\right] \mathrm{d}\kappa, 0 \le z \le z_D \\ \frac{8}{3}\pi^2 \int_0^\infty \kappa^3 \left[\left(\gamma_1 + \gamma_2 \frac{z_D + d_\varepsilon/2}{z}\right)\Phi_n^{(ocean)}(\kappa)\right. \\ \left. + \gamma_2 \frac{(z - z_D - d_\varepsilon/2)}{z}\Phi_n^{(air)}(\kappa)\right] \mathrm{d}\kappa, \\ z_D < z \le z_D + d_\varepsilon \\ \frac{8}{3}\pi^2 \int_0^\infty \kappa^3 \left[\frac{z_D + d_\varepsilon/2}{z}\Phi_n^{(ocean)}(\kappa)\right. \\ \left. + \frac{(z - z_D - d_\varepsilon/2)}{z}\Phi_n^{(air)}(\kappa)\right] \mathrm{d}\kappa,\ z_D + d_\varepsilon < z \end{cases} \tag{28}$$

Moreover, the angular spread can be represented as [17]

$$\theta_{sp}(z) \equiv \lim_{z\to\infty} \frac{w(z)}{z} = \sqrt{(\beta_x + \beta_y)/k^2 + \Theta z} \tag{29}$$

D. Rayleigh Range

The Rayleigh range z_R characterizes the collimation interval of the beam, defined as the propagation distance hen the cross-sectional area of the beam reaches twice at the field source [32], and z_R can be expressed as:

$$w^2(z_R) = 2w^2(0) \tag{30}$$

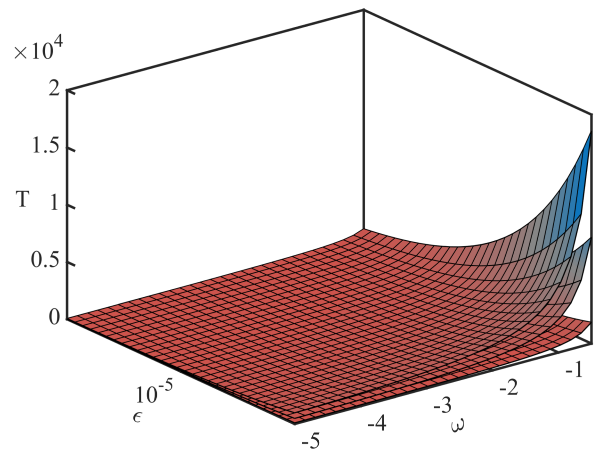

Fig. 2. Diagram of beam width versus the oceanic parameters.

Bring formula (23) into formula (30), and we can obtain

$$z_R = \frac{1}{3\gamma}\left(\Im + \frac{\beta^2}{\Im} - \beta\right) \tag{31}$$

where

$$\Im = \left[\frac{27}{2}\alpha\Theta^2 - \beta^3 + \frac{3}{2}\Theta\left(81\alpha^2\Theta^2 - 12\alpha\beta^3\right)^{1/2}\right]^{1/3} \tag{32}$$

and $\alpha = \alpha_x + \alpha_y, \beta = \frac{\beta_x+\beta_y}{k^2}$.

III. Numerical Result

In the following, the results are presented in Figs. 2–6. Unless otherwise specified, the simulation parameters are selected as: $M = N = 7$, $x_d = y_d = 3$ cm, $\lambda = 0.54$ um, $w_0 = 1$ cm, $m = n = 4$, $\eta = 0.01$, $\alpha = 3.5$, ${C_n}^2 = 10^{-14}$, $d_\varepsilon = 5$ m, respectively. To compare the intensity of oceanic turbulence with that of atmospheric turbulence, we introduce parameter T ($T = \int_0^\infty \kappa^3\Phi_n^{(ocean)}(\kappa)\mathrm{d}\kappa/\int_0^\infty \kappa^3\Phi_n^{(air)}(\kappa)\mathrm{d}\kappa$) as a factor that represents the relative contribution of oceanic and atmospheric turbulence. The surfaces in Fig. 2 represent the values of T corresponding to χ_T is 10^{-8}, 5×10^{-8} and 10^{-7}, from the bottom to the top, respectively. It illustrates that T increases with the increase of χ_T and the decrease of ω and ε. That means the larger χ_T or the smaller ω and ε are, the stronger the oceanic turbulence is. In the rest part, we will use different values of T to represent different intensities of the ocean turbulence.

A. Mean Squared Beam Width

Fig. 3 presents the changes in the mean squared beam width of RHGABs at various propagation distances and turbulence intensities. Notably, in Fig. 3(a), the mean square beam width expands with the increase of propagation distance, whether in the atmosphere or ocean. At the distance of 50 m, an inflection point appears, which is exactly the distance from seawater-air interface to the initial plane. In general, oceanic turbulence has a greater impact on the variation of beam width corresponding to the atmospheric turbulence.

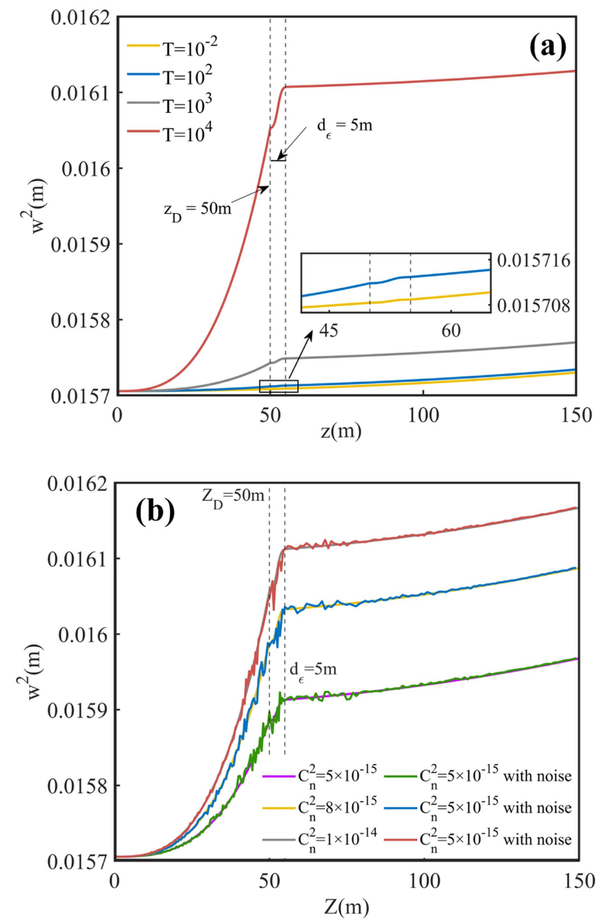

Fig. 3. Diagram of mean squared beam width versus propagation distance.

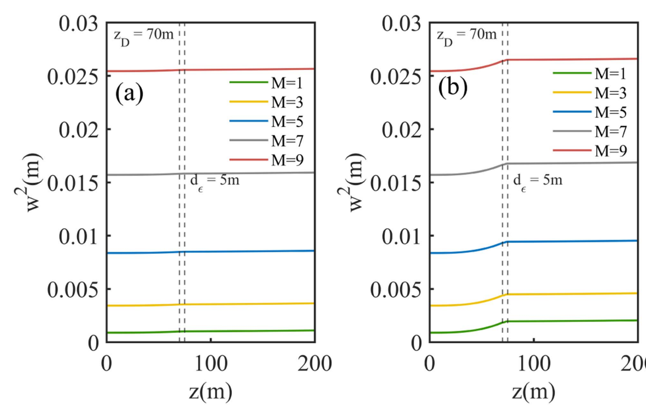

Fig. 4. Diagram of mean squared beam width versus the beam number and propagation distance ($M = N$).

Additionally, in Fig. 3(b), the overall trend of the mean square beam width considering environmental noise is basically consistent with that ignoring environmental noise. At the seawater-air interface, however, the random fluctuations on the mean squared beam width occur when this model considers environmental noise. It means that the environmental noise is a noteworthy and important factor for seawater-to-air optical communication.

Fig. 4 depicts the relationship between the beam width and beam number for varying values of T. Specifically, the values of

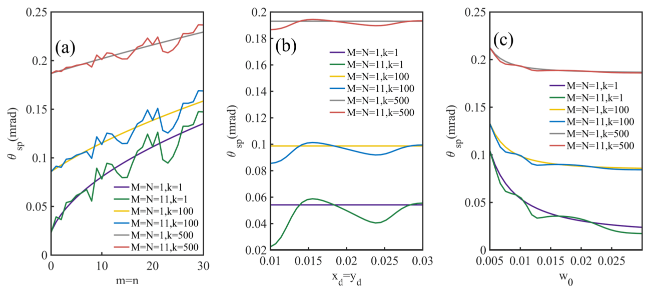

Fig. 5. Diagram of angular spread versus beam number, separated distance, and initial beam width.

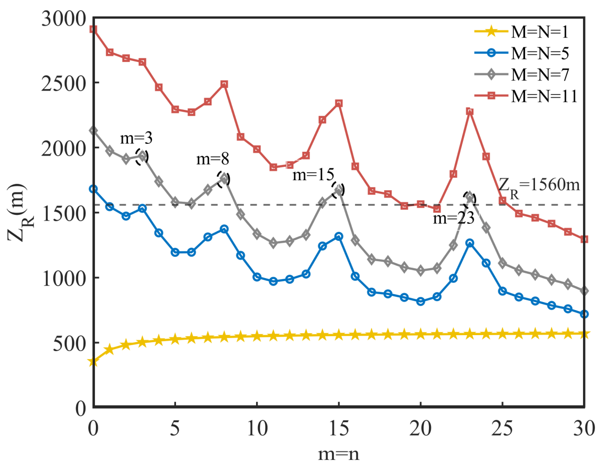

Fig. 6. Diagram of Rayleigh range versus beam order and beam number.

T in Fig. 4(a) and (b) are 1000 and 10000, respectively. These figures suggest that the larger value of k leads to faster beam width growth in the ocean, and greater contribution to overall propagation. The beam number plays a key role in the mean squared beam width, as a larger beam number results in a larger initial beam width, leading to a wider mean squared beam width in the propagation path.

B. Angular Spread

Fig. 5 illustrates the relationship between angular spread and RHGABs parameters (beam number, separated distance, initial beam width) under the conditions of atmospheric and oceanic turbulence, with a particular focus on the difference between single-beam and array beams. In Fig. 5(a), the impact of beam order on angular spread is depicted, the single-beam's angular spread increases as beam order increases. Fig. 5(b) shows that the angular spread remained constant for the single-beam as there is no distance variation between it and the adjacent beams. Fig. 5(c) reveals that the angular spread of the single-beam decreases with the increase of w_0. Generally, the variation of the single beam is monotonic, while it is opposite for the array beams. The angular spread of array beams oscillates along with the single beam for different m, x_d, and w_0. Additionally, it is important to note that a larger turbulence intensity corresponds to a larger angular spread and a smaller amplitude of oscillation.

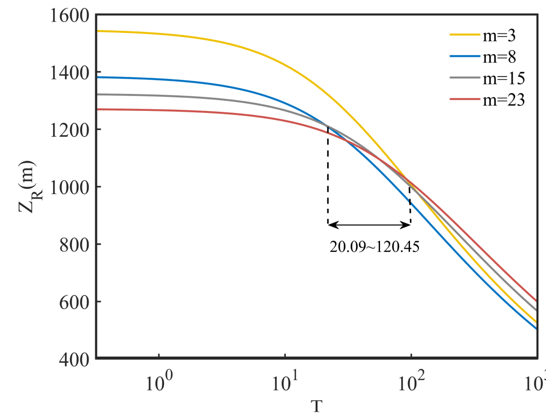

Fig. 7. Diagram of Rayleigh range versus beam order and relative contribution of oceanic and atmospheric turbulence.

C. Rayleigh Range

To examine the correlation between the Rayleigh range and the beam order, beam number, we present Fig. 6. The gray dashed line represents the threshold. Here, the threshold is set as the Rayleigh range when m, n take the values of $m = n = 5$. As depicted, the Rayleigh range increases with the increase of beam order in the case of single beam. Conversely, in the case of multiple beams, the Rayleigh range oscillates with the increase of the beam order. Moreover, the peak values of Rayleigh range appear at the beam order of 3, 8, 15, and 23, but the overall trend is downward. In addition, the Rayleigh range expands with the beam number, at the same beam order.

Fig. 7 shows that the Rayleigh range decreases with the increase of relative turbulence intensity T. It is of interesting that the Rayleigh range does not always decrease with the increase of the beam under the determined value of T. This phenomenon is consistent with the results in Fig. 6. It also can be reflected on the intersection of the curves in Fig. 7.

IV. Conclusion

In this paper, the propagation characteristics of RHGABs propagating through oceanic and atmospheric turbulence are studied. In the analytical model, we investigate the variation tendencies of Rayleigh range and angular spread. Our findings are as follows: the Rayleigh range increases with beam number under the same beam order. Moreover, the mean squared beam width increases more rapidly in oceanic turbulence than in the atmosphere. Furthermore, the angular spread of the RHGABs increases with the increase of the beam order. According to the above-mentioned results, one can increase the beam number to extend the effective communication distance. The conclusions in this paper are valuable for real optical communication system design.

Disclosures: The authors declare no conflicts of interest.

References

[1] M. V. Jamali et al., "Statistical studies of fading in underwater wireless optical channels in the presence of air bubble, temperature, and salinity random variations (Long Version)," *IEEE Trans. Commun.*, vol. 66, no. 10, pp. 4706–4723, Oct. 2018.

[2] L. Zhu et al., “Adaptive optics for orbital angular momentum-based internet of underwater things applications,” *IEEE Internet Things J.*, vol. 9, no. 23, pp. 24281–24299, Dec. 2022.

[3] L. Zhu, H. Yao, J. Wang, Q. Tian, Q. Zhang, and L. Hanzo, “Channel modeling for orbital angular momentum based underwater wireless optical systems,” *IEEE Trans. Veh. Technol.*, vol. 71, no. 6, pp. 5880–5895, Jun. 2022.

[4] Y. Li, Y. Zhang, and Y. Zhu, “Lommel-Gaussian pulsed beams carrying orbital angular momentum propagation in asymmetric oceanic turbulence,” *IEEE Photon. J.*, vol. 12, no. 1, Feb. 2020, Art no. 7900915.

[5] L. Zhu et al., “Security enhancement for adaptive optics aided longitudinal orbital angular momentum multiplexed underwater wireless communications,” *Opt. Exp.*, vol. 30, no. 6, pp. 9745–9772, 2022.

[6] G. Huang, L. Zhang, and Y. Jiang, “A general orthogonal transform aided MIMO design for reliable maritime visible light communications,” *J. Lightw. Technol.*, vol. 38, no. 23, pp. 6549–6560, Dec. 2020.

[7] L. Dou, X. Ji, and P. Li, “Propagation of partially coherent annular beams with decentered field in turbulence along a slant path,” *Opt. Exp.*, vol. 20, no. 8, pp. 8417–8430, 2012.

[8] C. Arpali, S. A. Arpali, and Y. Baykal, “Intensity fluctuations of partially coherent laser beam arrays in weak atmospheric turbulence,” *Appl. Phys.*, vol. 103, pp. 237–244, 2011.

[9] L. Lu, P. Zhang, and C. Fan, “Influence of oceanic turbulence on propagation of a radial Gaussian beam array,” *Opt. Exp.*, vol. 23, no. 3, pp. 2827–2836, 2015.

[10] D. Liu, Y. Wang, and H. Yin, “Evolution properties of partially coherent flat-topped vortex hollow beam in oceanic turbulence,” *Appl. Opt.*, vol. 54, pp. 10510–10516, 2015.

[11] Y. Q. Wu, Y. X. Zhang, and Y. Li, “Beam wander of Gaussian-Schell model beams propagating through oceanic turbulence,” *Opt. Commun.*, vol. 371, pp. 59–66, 2016.

[12] C. Y. Young, Y. V. Gilchrest, and B. R. Macon, “Turbulence induced beam spreading of higher order mode optical waves,” *Opt. Eng.*, vol. 41, no. 5, pp. 1097–1103, 2002.

[13] H. T. Eyyuboglu and Y. Baykal, “Hermite-Sine-Gaussian and Hermite-Sinh-Gaussian laser beams in turbulent atmosphere,” *Opt. Soc. Amer. J.*, vol. 22, no. 12, pp. 2709–2718, 2005.

[14] Y. Wang, J. Lian, and S. Gao, “Beam propagation factor of partially coherent elegant Hermite-Cosh-Gaussian beam through non-kolmogorov turbulence,” *Optik - Int. J. Light Electron Opt.*, vol. 125, no. 13, pp. 3166–3171, 2014.

[15] Ö. F. Sayan, H. Gerçekcioğlu, and Y. Baykal, “Hermite Gaussian beam scintillations in weak atmospheric turbulence for aerial vehicle laser communications,” *Opt. Commun.*, vol. 458, 2020, Art. no. 124735.

[16] Y. S. Yuan, Y. J. Cai, J. Qu, H. T. Eyyuboğlu, and Y. Baykal, “Propagation factors of Hermite–Gaussian beams in turbulent atmosphere,” *Opt. Laser Technol.*, vol. 42, no. 8, pp. 1344–1348, 2010.

[17] P. Zhu et al., “Propagation of a radially polarized Hermite-Cos-Gaussian correlated Schell-model beam in oceanic turbulence,” *Optik*, vol. 273, 2023, Art. no. 170487.

[18] Y. Li, L. Yu, and Y. Zhang, “Influence of anisotropic turbulence on the orbital angular momentum modes of Hermite-Gaussian vortex beam in the ocean,” *Opt. Exp.*, vol. 25, no. 11, pp. 12203–12215, 2017.

[19] G. Zhou, T. Zhou, F. Wang, R. Chen, Z. Mei, and X. Li, “Properties of airy transform of elegant Hermite-Gaussian beams,” *Opt. Laser Technol.*, vol. 140, 2021, Art. no. 107034.

[20] X. Wu, C. Wang, Y. Kong, and K. Wu, “Beam intensity and spectral coherence of Hermite-Cosine-Gaussian rectangular multi-Gaussian correlated Schell-model beam in oceanic turbulence,” *Heliyon*, vol. 9, no. 8, 2023, Art. no. e18374.

[21] Z. Cui, P. Yue, and Y. Xiang, “Beam wander in wireless optical communications between misaligned transceivers in oceanic turbulence,” *J. Opt. Soc. Amer. A*, vol. 37, no. 3, pp. 466–475, 2020.

[22] Z. L. Zhou and J. Qu, “Self-splitting and propagation factors of a superimposed Hermite-Gaussian correlated Schell-model beam in turbulent atmosphere,” *Results Phys.*, vol. 28, 2021, Art. no. 104609.

[23] X. Yi, Z. Li, and Z. Liu, “Underwater optical communication performance for laser beam propagation through weak oceanic turbulence,” *Appl. Opt.*, vol. 54, no. 6, pp. 1273–1278, 2015.

[24] V. V. Nikishov and V. I. Nikishov, “Spectrum of turbulent fluctuations of the sea-water refraction index,” *Int. J. Fluid Mechanics Res.*, vol. 27, no. 1, pp. 82–98, 2000.

[25] O. Korotkova and N. Farwell, “Intensity and coherence properties of light in oceanic turbulence,” *Opt. Commun.*, vol. 285, no. 6, pp. 872–875, 2012.

[26] O. Korotkova and N. Farwell, “Effect of oceanic turbulence on polarization of stochastic beams,” *Opt. Commun.*, vol. 284, no. 7, pp. 1740–1746, 2011.

[27] X. Chu, “Evolution of beam quality and shape of Hermite-Gaussian beam in non-Kolmogorov turbulence,” *Prog. Electromagn. Res.*, vol. 120, pp. 339–353, 2011.

[28] L. C. Andrews and R. L. Phillips, *Laser Beam Propagation Through Random Media*, 2nd ed. Bellingham, WA, USA: SPIE Press, 2005.

[29] X. Li and X. Ji, “Angular spread and directionality of the Hermite-Gaussian array beam propagating through atmospheric turbulence,” *Appl. Opt.*, vol. 48, no. 22, pp. 4338–4347, 2009.

[30] H. Tang, B. Ou, and B. Luo, “Average spreading of a radial Gaussian beam array in non-kolmogorov turbulence,” *J. Opt. Soc. Amer. A Opt. Image Sci. Vis.*, vol. 28, no. 6, pp. 1016–1021, 2011.

[31] M. Tang and D. Zhao, “Regions of spreading of Gaussian array beams propagating through oceanic turbulence,” *Appl. Opt.*, vol. 54, no. 11, pp. 3407–3411, 2015.

[32] A. E. Siegmann, *Lasers*. Sausalito, CA, USA: Univ. Sci. Books, 1986.